Assessment of Tracheal Stenosis Using Active Shape Models of Healthy Tracheas: A Surface Registration Study

Rômulo Pinho[1], Kurt Tournoy[2], Robert Gosselin[3], and Jan Sijbers[1]

[1] University of Antwerp, Department of Physics, VisionLab, Belgium
[2] Ghent University Hospital, Department of Respiratory Medicine, Belgium
[3] Ghent University Hospital, Department of Radiology, Belgium
{romulo.pinho, jan.sijbers}@ua.ac.be;
kurt.tournoy@ugent.be; robert.gosselin@uzgent.be

Abstract. Tracheal stenosis is a life threatening condition for which the successful treatment relies on the precise evaluation of its dimensions and severity. Recently, Active Shape Models (ASMs) were proposed for stenosis assessment and stent prediction, with promising results. An effective ASM, however, depends on the applied surface registration technique, which should not be influenced by the stenotic regions. The present work reviews previously proposed registration techniques and formulates a new method to estimate the shape of the healthy trachea of a patient with stenosis. Experiments with real and simulation data showed that the new method outperforms the conventional methods with respect to registration accuracy.

1 Introduction

Tracheal stenosis is a stricture of the windpipe that can be life threatening. Reconstruction or resection surgeries and the use of stents are important resources in the management of the condition. However, a successful treatment relies on the correct assessment of the stricture, which determines its location, length and degree of severity. Manual and computer aided approaches for the assessment of stenosis have been described in the literature [1–3].

Concomitantly, Active Shape Models (ASM) have been an important tool in computer aided diagnoses. In order to register the models to clinical data, the sum of the square of residuals between the model and the target is iteratively minimised. A problem may arise if the distribution of the residuals is not Gaussian, since standard least squares minimisation applied to non-Gaussian data distributions is known to be suboptimal. Deviations from Gaussian assumptions are normally evidenced by the presence of outliers in the data.

With the above concepts in mind, Pinho *et al.* claimed that correct assessment of stenosis depends on a good estimation of the healthy trachea of a patient and they used ASMs of tubular approximations of healthy tracheas for assessment of stenosis and prediction of stent dimensions [4]. The challenge in this approach, however, is to avoid the influence of stenotic regions on the registration of the ASM to clinical data. For this, they used a method in which, at each iteration, residuals corresponding to shape landmarks over regions with stenosis have their influence on the registration reduced by keeping these landmarks fixed w.r.t. the shape obtained in the previous iteration. Eventually, the fixed landmarks act as a counterforce against the attraction of stenotic regions, aiding the model in producing the desired healthy trachea.

Despite the promising results, the work above lacked a thorough analysis of the surface registration mechanism and experiments with clinical data. In the present work, we build upon [4], concentrating on the surface registration step of the ASM, and add the following contributions:

– formulate *FixedLandmarks* as a new method to avoid the influence of misleading regions during the registration of ASMs;
– build the ASM using correspondence optimisation of landmarks, as proposed by Huysmans *et al.* [5], instead of the tubular approximations used in [4];
– investigate the behaviour of *FixedLandmarks* and other methods through a comprehensive set of experiments on clinical as well as on simulation data;
– present qualitative and quantitative comparisons between the registration methods and standard least squares with respect to the estimation of the healthy trachea.

We begin this paper with a review of ASMs and their use in the estimation of healthy tracheas, in Section 2. In Section 3, the registration mechanism and methods previously used with ASMs are briefly described before the formulation of the *FixedLandmarks*. In Section 4, the experiments and results are presented and the article is concluded in Section 5.

2 Active Shape Model of Healthy Tracheas

ASMs are built from a training set of N aligned shapes, $\mathbf{x}_i$, each represented by the concatenation of its n, d-dimensional landmarks, which must correspond across the training set. Principal Component Analysis then extracts the N eigenvectors and non-negative eigenvalues of the covariance matrix of the training set. New shapes $\mathbf{x}$ are obtained with a linear combination between the average shape of the training set, $\overline{\mathbf{x}}$, and the $dn \times N$ matrix of orthonormal eigenvectors, $\mathbf{P}$:

$$\mathbf{x} = \overline{\mathbf{x}} + \mathbf{P}\mathbf{b} \ , \tag{1}$$

where $\mathbf{b}$ is an $N \times 1$ vector of weights, which are the parameters of the model [6].

ASMs can be registered to an object of the class they represent by adjusting the parameter set $\mathbf{b}$. When the model is applied to an image, the registration is usually an iterative process: the landmarks of the shape generated by the model at the current iteration are moved along their normals, generating a candidate shape $\mathbf{y}$, which matches high gradients corresponding to edges of the target. Afterwards, a new set of parameters $\hat{\mathbf{b}}$ is computed in order to allow the model to be registered to $\mathbf{y}$. The set $\hat{\mathbf{b}}$ which defines the best fit of the model to the candidate shape is obtained by minimisation of the squared error between $\mathbf{y}$ and $\mathbf{x}$, represented by the following error function:

$$\xi(\mathbf{b}) = (\mathbf{y} - \mathbf{x})^T(\mathbf{y} - \mathbf{x}) \ . \tag{2}$$

Expanding Eq. (2) with Eq. (1) and minimising ξ with respect to $\mathbf{b}$ results in:

$$\hat{\mathbf{b}} = \mathbf{P}^T(\mathbf{y} - \overline{\mathbf{x}}) \ . \tag{3}$$

This minimisation is herein referred to as *StandardLS*. This whole procedure is repeated until no significant changes have been made to the shape generated by the model at subsequent iterations.

Huysmans *et al.* proposed a method for shape modelling of cylindrical surfaces using cylindrical parametrisation [5]. In their method, the shapes of the training set are first aligned using the iterative closest point algorithm [7] and mapped on the unit cylinder, with a criterion to minimise distortions. The choice of landmarks along the boundaries of the shapes is made automatically, in the parametric domain. Likewise, the correspondences between the landmarks are established in the parametric domain, using minimum description length [8]. The optimised landmarks are later mapped back onto the original shapes. The boundary shapes, $\mathbf{x}_i$, are eventually described by the concatenation of n landmarks $\mathbf{x}_{\mathrm{v}_j} = (x_j, y_j, z_j)$ and used to build the model.

As shown in [6], shapes generated with ASMs resemble those in the training set. By constructing the model with healthy tracheas only, local distortions typical of stenotic geometry are not present. As a result, the edges in the image corresponding to regions with stenosis have low impact on local deformations of the ASM. Yet, the shape generated by the model can still be globally narrowed. In order to cope with this drawback, the registration is divided into two iterative stages. The first stage, a rigid registration, aligns the average shape of the model to the target trachea. This procedure aids the gradient based search in finding the location and orientation of the target trachea. In addition, landmarks of the shape generated by model which are located in the vicinity of regions with stenosis tend to remain far from their corresponding target. In the second, non-rigid registration stage, those landmarks are kept fixed at each iteration in order to minimise their influence on the adjustment of the model parameters. As the shape generated by the model iteratively deforms, the expected result is a trachea that matches the healthy regions of the target and produces an estimation for the healthy caliber of its narrowed parts.

3 Surface Registration

When the distribution of the residuals, $\{r_j | j = 1, \ldots, n\}$, between $\mathbf{x}$ and $\mathbf{y}$ in Eq. (2) is not Gaussian, due to the presence of outliers, *StandardLS* may produce suboptimal results. The literature presents different approaches to avoid the influence of outliers. In the remainder of this section, we review some of these approaches applied to ASMs and formulate a new one, called *FixedLandmarks*.

Weighted Least Squares The influence of outliers can be reduced by assigning weights to the contribution of each residual, modifying Eq. (2) to

$$\xi_w(\mathbf{b}) = (\mathbf{y} - \mathbf{x})^T \mathbf{W}(\mathbf{y} - \mathbf{x}) \ , \tag{4}$$

where $\mathbf{W}$ is a diagonal matrix of weights. Minimising ξ_w with respect to $\mathbf{b}$ yields

$$\hat{\mathbf{b}} = (\mathbf{P}^T \mathbf{W} \mathbf{P})^{-1} \mathbf{P}^T \mathbf{W}(\mathbf{y} - \overline{\mathbf{x}}) \ , \tag{5}$$

which is the basic formulation of weighted least squares (*WLS*) minimisation.

From the above definition, it is clear that a good choice of weights is key for an effective use of *WLS*. In the field of Robust Statistics, estimators that are less affected by deviations from Gaussian or other model assumptions can be devised to further improve the effects of *WLS* [9]. Rogers *et al.* used robust statistics with ASMs in different medical applications and filled matrix $\mathbf{W}$ with the Huber weighting function [10]. Theobald *et al.* compared several weighting functions for landmark occlusion detection, among which the Talwar, the Cauchy, and the Gaussian weighting functions performed best [11]. Fig. 1 shows the four functions described. In all of them, σ is the standard deviation of the residuals, which can be estimated at each iteration from the median of their absolute values [10].

$$w_{\text{huber}_i} = \begin{cases} 1, & r_i < \sigma \\ \sigma/|r_i|, & \sigma \leq r_i < 3\sigma \\ 0, & r_i \geq 3\sigma \end{cases} \qquad w_{\text{talwar}_i} = \begin{cases} 1, & r_i < \sigma \\ 0, & r_i \geq \sigma \end{cases}$$

$$w_{\text{cauchy}_i} = \frac{1}{1 + \left(\frac{r_i}{\sigma}\right)^2} \qquad w_{\text{gauss}_i} = \frac{1}{\sigma\sqrt{2\pi}} e^{-\frac{(r_i-\mu)^2}{2\sigma^2}}$$

Fig. 1. Huber, Talwar, Cauchy, and Gaussian weighting functions.

In the present work, we assume that the rigid registration stage of the ASM, as described in Section 2, results in a shape near healthy regions of the trachea and far from narrowed ones. Therefore, according to the definitions above, the r_i's corresponding to landmarks over these narrowed regions will be considered the outliers in the distribution.

Surface Extrapolation In this approach, the purpose is to use the model to predict missing parts of the target shape. At each iteration k of the registration, $\mathbf{y}^{(k)} \approx (\overline{\mathbf{x}} + \mathbf{P}\hat{\mathbf{b}}^{(k)})|_{\mathcal{L}}$, where $\mathcal{L}$, of size m, denotes the set of landmarks of the model actually used. It is possible that $m \ll n$, where n is the total number of landmarks of the model. The parameter set $\hat{\mathbf{b}}^{(k)}$ is computed as in Eq. (2), but using only the components of $\mathbf{P}$ and $\mathbf{x}$ corresponding to the m target landmarks.

Rajamani *et al.* used extrapolation to predict the shape of the femur from manually sampled points during hip surgery [12]. In their method, the m sampled points are matched to the nearest landmarks of the shape generated by the model at each iteration. Furthermore, a weighting term added to the error function restricts the deformation freedom of the ASM as m decreases, forcing the model to produce shapes similar to the average shape. In [13], extrapolation was used to plan reconstructions of mandibular dysplasia. The ASM is registered to parts of the mandible that are considered as being regularly shaped.

Again, we assume that the shape generated by the rigid registration converges to a location near healthy regions of the trachea and far from those with stenosis. Thus, the set $\mathcal{L}$ will represent landmarks associated to healthy regions, to which the ASM is expected to yield the best possible match.

Fixed Landmarks Here we formulate a new registration technique, which we refer to as *FixedLandmarks*.

After the rigid registration, the landmarks of the shape generated by the model at the current iteration are displaced along their normals. If a high gradient is not found within a threshold distance $d > 0$, the corresponding landmarks remain fixed, while other landmarks are allowed to move as usual.

Let then $\mathbf{x}^{(k)} = \overline{\mathbf{x}} + \mathbf{P}\mathbf{b}^{(k)}$ be the shape generated with the model at any iteration k of the non-rigid registration. Let $\mathbf{y}^{(k+1)}$ be the candidate shape generated by displacing the landmarks of $\mathbf{x}^{(k)}$ and let $d\mathbf{y}^{(k+1)} = \mathbf{y}^{(k+1)} - \mathbf{x}^{(k)}$. As described in the previous paragraph, if $\|\mathbf{y}^{(k+1)}_{\mathrm{v}_j} - \mathbf{x}^{(k)}_{\mathrm{v}_j}\| > d$, then $\mathbf{y}^{(k+1)}_{\mathrm{v}_j} = \mathbf{x}^{(k)}_{\mathrm{v}_j}$ and $d\mathbf{y}^{(k+1)}_{\mathrm{v}_j} = \mathbf{0}$, where $j = 1 \ldots n$. In other words, some landmarks of the candidate shape $\mathbf{y}^{(k+1)}$ remain fixed w.r.t. $\mathbf{x}^{(k)}$. Grouping the $d\mathbf{y}^{(k+1)}_{\mathrm{v}_j} = \mathbf{0}$ and the corresponding columns of $\mathbf{P}^T$ results in two subsets of landmarks, $\mathcal{L}'$ and $\mathcal{L}''$, of sizes n' and n'', respectively, such that $d\mathbf{y}^{(k+1)}|_{\mathcal{L}''} = \mathbf{0}$. Let us then write

$$\hat{\mathbf{b}}^{(k+1)} = \mathbf{P}^T(\mathbf{x}^{(k)} + d\mathbf{y}^{(k+1)} - \overline{\mathbf{x}}) \ , \tag{6}$$

from Eq. (3), and split it into

$$\hat{\mathbf{b}}^{(k+1)} = \left[\mathbf{P}^T(\mathbf{x}^{(k)} + d\mathbf{y}^{(k+1)} - \overline{\mathbf{x}})\right]\Big|_{\mathcal{L}'} + \left[\mathbf{P}^T(\mathbf{x}^{(k)} + d\mathbf{y}^{(k+1)} - \overline{\mathbf{x}})\right]\Big|_{\mathcal{L}''} \ , \tag{7}$$

which does not affect the result. Since $d\mathbf{y}^{(k+1)}|_{\mathcal{L}''} = \mathbf{0}$, we finally obtain

$$\hat{\mathbf{b}}^{(k+1)} = \left[\mathbf{P}^T(\mathbf{y}^{(k+1)} - \overline{\mathbf{x}})\right]\Big|_{\mathcal{L}'} + \left[\mathbf{P}^T(\mathbf{x}^{(k)} - \overline{\mathbf{x}})\right]\Big|_{\mathcal{L}''} \ , \tag{8}$$

showing that $\hat{\mathbf{b}}^{(k+1)}$ is determined by both the displaced landmarks $\mathbf{y}^{(k+1)}|_{\mathcal{L}'}$ and the landmarks $\mathbf{x}^{(k)}|_{\mathcal{L}''}$, which remained fixed[1]. Consequently, when computing

$$\hat{\mathbf{x}}^{(k+1)} = \overline{\mathbf{x}} + \mathbf{P}\hat{\mathbf{b}}^{(k+1)} \ , \tag{9}$$

[1] Note that $\mathcal{L}'$ and $\mathcal{L}''$ can be different at each iteration.

$\hat{\mathbf{x}}^{(k+1)}$ will be the best fit, in a least squares minimisation sense, to $\mathbf{y}^{(k+1)}|_{\mathcal{L}'}$ and $\mathbf{x}^{(k)}|_{\mathcal{L}''}$. Provided that there are enough healthy areas around regions with stenosis, the fixed landmarks force the shape generated by the model to remain far from those regions, while enabling correct matches at the healthy areas. As the shape deforms iteratively, it progressively assumes the form of the desired healthy trachea, guided by the regions where correct matches occur.

4 Experiments

We carried out experiments on simulation as well as on clinical data in order to compare the different registration techniques discussed in Section 3. With the simulation data, ground truths were formally established and the experiments provided a reliable quantitative comparison between the registration techniques. The experiments with clinical data, in turn, provided a qualitative comparison between them.

To build the ASM, we used $N = 9$ healthy tracheas at total lung capacity, each with $n = 1024$ landmarks. The low-dose, chest CT scans of their respective patients were obtained from pulmonary medication studies carried out at the University Hospital of Antwerp, Belgium, and patient data were anonymised before the images were used. The tracheas were segmented from the images using a region growing algorithm dedicated to the segmentation of the airways [14] and then converted to a 3-dimensional shape with the marching cubes algorithm [15]. The 3-d shapes were later supplied to the correspondence optimisation algorithm, as in Section 2, which eventually produced the shapes used in the model.

4.1 Quantitative Comparison

In order to quantitatively compare the registration methods, we ran a large set of leave-one-out tests using simulation data. First, for each of the N healthy tracheas, 72 phantoms of stenosis – 24 anteriorly located (A), 24 posteriorly (P), and 24 roughly symmetrically narrowed (S) – were created. The stenotic areas were generated by applying a local erosion mask to the binary images of the segmented healthy tracheas until the stenosis achieved the desired shape [4]. The phantoms followed the categories of Fig. 2, based on [16], and were validated by an expert in the pulmonology field. For example, phantom I-1P represents a posterior stenosis of less than 25% along the upper third of the trachea.

For each run of the $T = N$ leave-one-out tests, the model was built with $N-1$ tracheas and was then registered to the phantoms created from the trachea not present in the training set. In all tests, the average shape of the ASM was initially roughly placed near the target trachea in the image. Moreover, the non-rigid registration methods were only triggered after the convergence of the rigid registration. Since the initial conditions were always the same, our evaluation is guaranteed to be fair.

The quality of the assessment of stenosis using the ASM strongly depends on the estimation of the healthy trachea of the patient. Therefore, the objective of this set of experiments is to register the model to the phantoms using all the registration methods and to measure the distance between the estimated tracheas and their originally healthy counterparts. For this purpose, we employed the algorithm proposed in [17] to compute errors between surfaces using the Hausdorff distance.

The iteration limit for the registration was set to 200. The minimum squared error between shapes generated at subsequent iterations, i.e., $\xi_{\mathrm{r}}^{(k)} = (\mathbf{x}^{(k)} - \mathbf{x}^{(k-1)})^T(\mathbf{x}^{(k)} - \mathbf{x}^{(k-1)})$, was set to $10^{-7}\mathrm{mm}^2$. In the *FixedLandmarks*, the landmarks were displaced within a distance $d = 1$mm along their normals. For the *Surface Extrapolation*, the m landmarks of the candidate shape that guided the deformations were those that remained near the target surface ($d \leq 1$mm) after each iteration of the registration. In addition, we dropped the weighting term defined in [12], since shapes similar to the average shape of the model are very unlikely to produce a good estimation of a specific healthy trachea. In this way, the *Surface Extrapolation* becomes equivalent to using *WLS* with a step function yielding binary weights. Besides the robust approaches of Section 3, we also included in the comparison the *StandardLS*, i.e., not distinguishing between healthy and stenotic areas on the target surfaces. In total, we ran 4536 tests.

4.2 Qualitative Comparison

In addition to the simulation experiments, we made a retrospective study with chest CT scans from 3 patients. The use of the CT scans was approved by the ethics committee of the Ghent University Hospital (doc. ECUZG2009/140), Belgium, and patient data were anonymised before the images were used in the experiments. The 3 patients had stenosis with the following characteristics:

- Patient 1 had severe posterior stenosis along the lower half of trachea,
- Patient 2 had severe lateral stenosis along the two lower thirds of the trachea,
- Patient 3 had severe symmetrical stenosis along the lower half of the trachea.

No preprocessing was applied to any of the 3-d CT images. In addition, they were very anisotropic in the axial direction, with pixel resolution, in mm, (0.62, 0.62, 3.00), (0.98, 0.98, 5.00), and (0.44, 0.44, 3.00) respectively.

Since the registration is an iterative, edge based search, neighbouring organs and structures as well as noise may mislead the search. Therefore, the registration

CATEGORY	LOCATION AND LENGTH
I	Upper third of the trachea
II	Middle third of the trachea
III	Lower third of the trachea
I-II	Upper third extending to middle third
II-III	Middle third extending to lower third
I-III	Upper third extending to lower third

CATEGORY	DEGREE
1	<25%
2	26–50%
3	51–75%
4	>75%

Fig. 2. Categories of stenosis based on location and length (L) and degree (R).

is dependent on the initial search location. At this point, the initialisation of the registration is done manually, by conveniently placing the average shape of the model inside the image, namely, near the target trachea. For each patient, the initial position of the model was manually set for one registration method, recorded, and then replicated for all other methods. The results were reviewed by an expert in the pulmonology field in order to qualitatively compare all methods with respect to the estimated healthy trachea.

The ASM built for these experiments contained all the $N = 9$ healthy tracheas. As before, the maximum number of iterations was set to 200, the minimum $\xi_{\mathrm{r}}^{(k)}$ was set to $10^{-7}\mathrm{mm}^2$, and $d = 1\mathrm{mm}$. *WLS* and *StandardLS* were used in the same way as in the experiments with simulation data.

4.3 Results and Discussion

For the quantitative comparison between the registration methods using the simulation data, we subdivided the phantoms of each healthy trachea into $G = 10$ groups, according to the categories defined in Fig. 2, each with a different size S_g. The reasoning behind this subdivision is to show how the methods behaved relative to variations in location, length, and degree of stenosis across the whole set of T leave-one-out tests. Let us then define, for a test instance t, $\delta_{\mathrm{max}_{gtp}}$ and $\delta_{\mathrm{mean}_{gtp}}$ as the maximum and mean distances, respectively, between the estimated trachea for phantom p, of group g, and its original, healthy equivalent. As stated in Section 4.1, these distances are obtained using the algorithm proposed in [17]. Afterwards,

$$\overline{\delta}_{\mathrm{max}_{gt}} = \frac{1}{S_g}\sum_{p=1}^{S_g}\delta_{\mathrm{max}_{gtp}} \text{ and } \overline{\delta}_{\mathrm{mean}_{gt}} = \frac{1}{S_g}\sum_{p=1}^{S_g}\delta_{\mathrm{mean}_{gtp}} \tag{10}$$

can be calculated as the average, per-group maximum and mean distances, respectively, for one test instance.

For the final comparison, we computed each group's average maximum error, μ_{max_g}, and average mean error, μ_{mean_g}, for each method, across the whole set of T leave-one-out tests. That is,

$$\mu_{\mathrm{max}_g} = \frac{1}{T}\sum_{t=1}^{T}\overline{\delta}_{\mathrm{max}_{gt}} \text{ and } \mu_{\mathrm{mean}_g} = \frac{1}{T}\sum_{t=1}^{T}\overline{\delta}_{\mathrm{mean}_{gt}} \quad . \tag{11}$$

The results and their respective standard deviation bars are shown in Fig. 3.

As expected, the *StandardLS* did not perform well. The influence of the stenotic regions on the registration indeed made the resulting shape much narrower or deformed than desired. The use of *WLS* brought some improvements, but not enough to completely remove the influence of stenotic regions. The problem with the weighting approaches is the difficulty in finding the proper weight assigning function to act only on the regions with stenosis. If the weighting scheme is too tight, the shape may not deform enough, remaining similar to

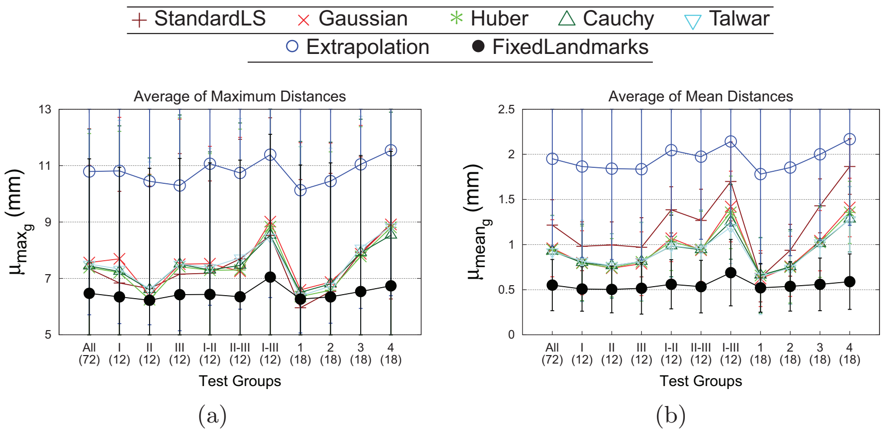

Fig. 3. Per-group $\mu_{\max_g}$ (a), μ_{mean_g} (b), and respective standard deviation bars for each method across the whole set of leave-one-out tests. Along the horizontal axis, the number of phantoms in the test group, S_g, is shown in parentheses.

the mean shape. If it is too loose, the shape may be strongly attracted by the areas with stenosis. Regarding the *Surface Extrapolation*, using only the points near the target surface to guide the deformations eventually resulted in few, very localised points, especially in the most severe cases. Without a stronger clue to indicate the shape to be obtained in a global level, the method could not converge to the desired result, which explains its poor performance. We can therefore conclude that the *FixedLandmarks* was the best registration method. It is especially worth noting how other methods performed worse as the length and degree of stenosis increased, while the *FixedLandmarks* was hardly affected. Its μ_{mean_g}'s remained near 0.5mm in all but one test group, I-III, which represented the longest and most severe types of stenosis in the simulation data.

Fig. 4 presents an example of the estimation of the healthy trachea for phantom II-4A generated from one of the healthy tracheas used in our experiments, using the *StandardLS*, *GaussWLS*, *HuberWLS*, *Surface Extrapolation*, and *FixedLandmarks* methods. The dashed, outermost silhouette in each case represents the original healthy trachea and the *FixedLandmarks* yielded the best fit to it.

As mentioned before, the results from the experiments with clinical data were reviewed by an expert in the pulmonology field. It can be seen in Fig. 5 that the *FixedLandmarks* produced very plausible healthy tracheas. They have an acceptable caliber and generally follow the curvature of the patient's trachea. Fig. 6 shows the results of other methods applied to the CT scan of patient 1. It can be seen how the severely narrowed trachea influenced the registration and either made the estimated tracheas too narrow and deformed or led them astray.

It is important to mention that the quality of the results obtained with the *FixedLandmarks* depends on the choice of the sets $\mathcal{L}'$ and $\mathcal{L}''$, which corresponds to landmarks that are allowed to move and those that remain fixed, respectively. These sets, in turn, depend on the choice of d. Intuitively, as d increases, the

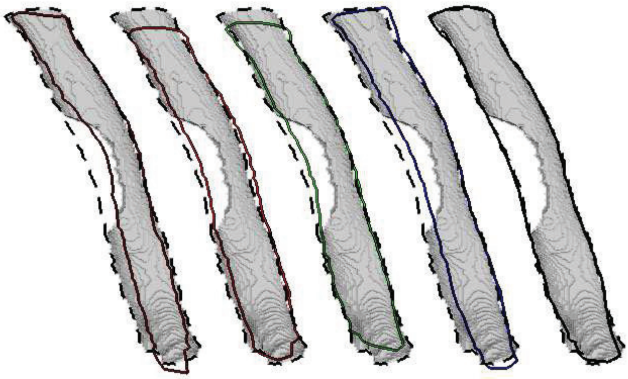

Fig. 4. Shape estimation for phantom II-4A of one healthy trachea from the simulation experiments, using, from left to right, the *StandardLS*, *GaussWLS*, *HuberWLS*, *Surface Extrapolation*, and *FixedLandmarks* methods. The dashed, outermost silhouettes represent the healthy trachea used to build the phantom.

FixedLandmarks tends to perform like the *StandardLS*, since $\mathcal{L}''$ will tend to be empty and no landmarks will remain fixed. The registration will thus not be guarded against the attraction of stenotic regions. If d is too short, $\mathcal{L}'$ will tend to be empty and, as opposed to the previous case, all landmarks will remain fixed. One option to solve this problem is to let this parameter be set by the user. Different values of d should then be tried until acceptable results are yielded. Another possibility is to devise an adaptive algorithm to change d as needed during the registration. Nevertheless, the value $d = 1$mm proved to be a good empirical choice in our comprehensive set of experiments.

The *FixedLandmarks* tended to fail when the rigid registration stage converged to a location where estimated healthy areas were either still far from the target trachea or too close to areas with stenosis. In the former case, the model shape was not attracted by the edges of the target. In the latter case,

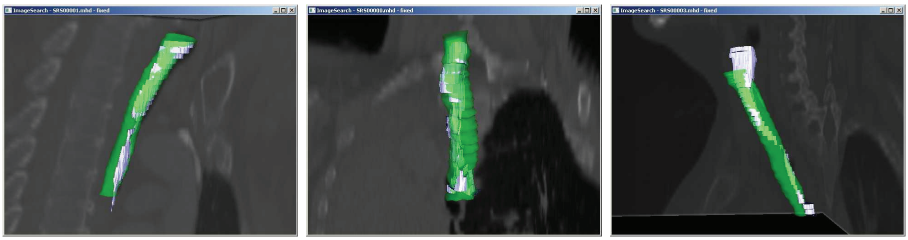

Fig. 5. Results of the estimation of the healthy trachea with the *FixedLandmarks* for patients 1, 2, and 3, from left to right. The estimated trachea, in green, is shown in the CT scan of the patient, overlaid on their segmented stenotic trachea.

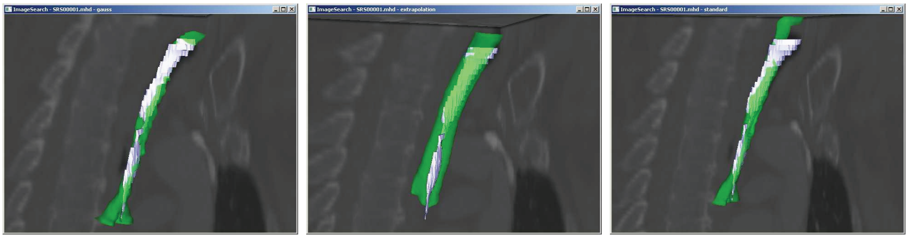

Fig. 6. *GaussWLS* (L), *Surface Extrapolation* (M), and *StandardLS* (R) registration methods applied to the CT scan of Patient 1. The estimated trachea, in green, is placed in the image, overlaid on the segmented stenotic trachea. With *Surface Extrapolation*, the estimated surface failed to match the lower part of the trachea. With other methods, the surface was too narrow or deformed.

the stenosis had stronger influence on the deformations, making the estimated shape somewhat narrower than desired. As stated above, the parameter d can be adjusted to try to reduce this problem, but further investigation of the rigid registration stage is still necessary.

Finally, we observed that problems with all approaches occurred mainly at areas where the shape of the trachea has more variation, namely the upper and lower thirds. This problem may be solved by an increase in the size and variability of the training set of the ASM and further experiments are ongoing[2].

5 Conclusion

We investigated the behaviour of registration methods used with Active Shape Models to estimate the healthy trachea of patients with tracheal stenosis. The estimated tracheas can be used, for instance, in surgery planning and prediction of stent dimensions. A new method, named *FixedLandmarks*, was formulated in order to avoid the influence of stenotic regions during the registration of the ASM to image data. The method works by keeping landmarks of the model associated to regions with stenosis fixed w.r.t. the previous iteration of the registration, which forces the shape generated by the model to stay far from these regions while enabling correct matches along healthy areas of the trachea. Experiments were carried out on simulation as well as on clinical data and the *FixedLandmarks* proved to be the best method when compared to other ones.

6 Acknowledgments

We thank the Pulmonology and the Radiology departments of the Ghent University Hospital and of the University Hospital of Antwerp for providing us with

[2] We refer the reader to http://www.youtube.com/user/fixedlandmarks for the latest results.

the images used in the experiments. We also thank the financial support of the IBBT (Interdisciplinary Institute for Broadband Technology), Belgium.

References

1. Carretta, A., Melloni, G., Ciriaco, P., Libretti, L., Casiraghi, M., Bandiera, A., ZanniniD, P.: Preoperative assessment in patients with postintubation tracheal stenosis. Surgical Endoscopy **20** (2006) 905–908
2. Kiesler, K., Gugatschka, M., Sorantin, E., Friedrich, G.: Laryngo-tracheal profile: a new method for assessing laryngo-tracheal stenoses. Eur Arch Otorhinolaryngol **264** (2007) 251–256
3. Shitrit, D., Valdsislav, P., Grubstein, A., Bendayan, D., Cohen, M., Kramer, M.: Accuracy of virtual bronchoscopy for grading tracheobronchial stenosis: correlation with pulmonary function test and fiberoptic bronchoscopy. Chest **128** (2005) 3545–3550
4. Pinho, R., Huysmans, T., Vos, W., Sijbers, J.: Tracheal stent prediction using statistical deformable models of tubular shapes. In: Proc. SPIE MI. (2008) 69144O
5. Huysmans, T., Sijbers, J., Vanpoucke, F., Verdonk, B.: Improved shape modeling of tubular objects using cylindrical parameterization. In: Proc. MIAR. Volume 4091. (2006) 84–91
6. Cootes, T.F., Taylor, C.J., Cooper, D.H., Graham, J.: Active shape models: their training and application. Comput. Vis. Image Underst. **61** (1995) 38–59
7. Besl, P.J., McKay, N.D.: A method for registration of 3-d shapes. IEEE Trans. Pattern Anal. Mach. Intell. **14** (1992) 239–256
8. Davies, R.H., Twining, C.J., Cootes, T.F., Waterton, J.C., Taylor, C.J.: 3d statistical shape models using direct optimisation of description length. In: Proc. ECCV Part III. (2002) 3–20
9. Huber, P.J.: Robust Statistics. Wiley (1981)
10. Rogers, M., Graham, J.: Robust active shape model search. In: Proc. ECCV Part IV. (2002) 517–530
11. Theobald, B.J., Matthews, I., Baker, S.: Evaluating error functions for robust active appearance models. In: Proc. IEEE FG. (2006) 149–154
12. Rajamani, K.T., Styner, M.A., Talib, H., Zheng, G., Nolte, L.P., Ballester, M.A.G.: Statistical deformable bone models for robust 3d surface extrapolation from sparse data. Medical Image Analysis **11** (2007) 99–109
13. Zachow, S., Lamecker, H., Elsholtz, B., Stiller, M.: Reconstruction of mandibular dysplasia using a statistical 3d shape model. In: Proc. CARS. Volume 1281. (2005) 1238–1243
14. Pinho, R., Sijbers, J., Vos, W.: Efficient approaches to intrathoracic airway tree segmentations. In: Proc. IEEE EMBS Benelux Symposium. Volume 2. (2006) 151–154
15. Lorensen, W.E., Cline, H.E.: Marching cubes: A high resolution 3d surface construction algorithm. SIGGRAPH Comput. Graph. **21** (1987) 163–169
16. Freitag, L., Ernst, A., Unger, M., Kovitz, K., Marquette, C.: A proposed classification system of central airway stenosis. Eur Respir J. **30** (2007) 7–12
17. Aspert, N., Santa-Cruz, D., Ebrahimi, T.: Mesh: Measuring errors between surfaces using the hausdorff distance. In: Proc. IEEE ICME. Volume I. (2002) 705–708